Conference paper

Andrea Scarperi, Noemi Landi, Alessio Gabbani, Nabila Jarmouni, Silvia Borsacchi, Lucia Calucci, Andrea Pucci, Elisa Carignani*, Francesco Pineider and Marco Geppi

Multinuclear solid state nuclear magnetic resonance for studying $CsPbBr_3$ nanocubes

https://doi.org/10.1515/pac-2023-0110

Abstract: Cesium lead bromide perovskite ($CsPbBr_3$) nanocrystals have raised impressive interest as efficient and stable optoelectronic materials. Size and morphology play important roles in the final performances of these materials and advanced characterization studies are needed to elucidate structural and surface properties. In this work, $CsPbBr_3$ cubic nanocrystals were obtained by colloidal synthesis and characterized by multinuclear Solid State NMR (SSNMR), complemented by X-Ray Diffraction (XRD), Transmission Electron Microscopy (TEM) and optical spectroscopy. The multinuclear NMR approach allowed the different components of the nanocubes to be separately observed. In particular, the surface ligands and their interactions with the nanocubes surface were investigated by ^{1}H and ^{13}C NMR experiments, while the structural investigation of the perovskite nanocubes was addressed by exploiting ^{207}Pb and ^{133}Cs spectral properties in comparison with bulk $CsPbBr_3$. Static ^{207}Pb NMR spectra indicated a possible contribution of chemical shift anisotropy from the ^{207}Pb nuclei of the outer layer. The ^{133}Cs NMR spectra showed signals with different chemical shifts for cesium atoms in at least three regions of the nanocubes, from the inner core to the surface, which were interpreted in terms of cubic layers with different distances from the surface using a simple geometrical model. This interpretation was also supported by ^{133}Cs longitudinal relaxation time measurements.

Keywords: ^{1}H NMR; ^{13}C NMR; ^{133}Cs NMR; ^{207}Pb NMR; Italian-French NMR conference; Magic Angle Spinning (MAS); nanocrystals; perovskites.

Introduction

The term perovskite indicates a class of ionic solids with general chemical formula ABX_3 that are isostructural to calcium titanate ($CaTiO_3$) [1]. In the last 20 years, metal halide perovskites (MHP) – where B is a divalent

Article note: "A collection of invited papers based on presentations at the Italian-French International Conference on Magnetic Resonance", Milan, Italy, 27–30 September 2022.

***Corresponding author: Elisa Carignani**, Institute for the Chemistry of Organometallic Compound, National Council of Research (ICCOM-CNR), via Moruzzi 1, 56124 Pisa, Italy, e-mail: elisa.carignani@pi.iccom.cnr.it. https://orcid.org/0000-0001-5848-9660

Andrea Scarperi, Noemi Landi, Andrea Pucci and Marco Geppi, Department of Chemistry and Industrial Chemistry, University of Pisa, via G. Moruzzi 13, 56124 Pisa, Italy. https://orcid.org/0009-0002-5089-4535 (N. Landi). https://orcid.org/0000-0003-1278-5004 (A. Pucci). https://orcid.org/0000-0002-2422-8400 (M. Geppi)

Alessio Gabbani and Francesco Pineider, Department of Chemistry and Industrial Chemistry, University of Pisa, via G. Moruzzi 13, 56124 Pisa, Italy; and Department of Physics and Astronomy, University of Florence, I-50019 Sesto Fiorentino (FI), Italy. https://orcid.org/0000-0002-4078-0254 (A. Gabbani). https://orcid.org/0000-0003-4066-4031 (F. Pineider)

Nabila Jarmouni, Department of Chemistry and Industrial Chemistry, University of Pisa, via G. Moruzzi 13, 56124 Pisa, Italy; and Department of Chemistry, Laboratory of Physical Chemistry of Materials, Faculty of sciences Ben M'sik, University Hassan II of Casablanca, Av Driss El Harti, Sidi Othmane Casablanca, B.P 7955, Casablanca, Morocco. https://orcid.org/0000-0002-0111-825X

Silvia Borsacchi and Lucia Calucci, Institute for the Chemistry of Organometallic Compound, National Council of Research (ICCOM-CNR), via G. Moruzzi 1, 56124 Pisa, Italy; and Center for Instrument Sharing of the University of Pisa (CISUP), 56124 Pisa, Italy. https://orcid.org/0000-0003-3696-0719 (S. Borsacchi). https://orcid.org/0000-0002-3080-8807 (L. Calucci)

metal, typically Pb^{2+}, Sn^{2+}, or Bi^{2+}, and X is a halide (Cl^-, Br^- or I^-) – have aroused a great interest for their applications in optoelectronics and especially for highly efficient photovoltaics [2]. Depending on the nature of the A cation, metal halide perovskites can be classified as *organic–inorganic* hybrid perovskites when A is an organic cation (typically methylammonium or formamidinium) or *all-inorganic* perovskites when A is an inorganic cation, e.g., Cs^+. Despite their amazing performances in photovoltaic devices, the applications of *organic–inorganic* hybrid perovskites are severely limited by their sensitivity to moisture, oxygen, and heat [3]. On the other hand, *all-inorganic* perovskites usually show higher thermo-stability [4].

With respect to bulk perovskites, MHP nanocrystals have higher photoluminescence quantum yields (PLQYs), narrower emission bandwidth, higher stability, and richer possibilities of surface functionalization [5]. These characteristics allowed their use in several applications, such as light-emitting diodes (LEDs) [6], lasers [7], spintronics [8], photovoltaics (reaching certified power conversion efficiency of 16.6 % [9]) and photocatalysis [10]. Moreover, as other semiconductors, nanocrystals of MHP exhibit quantum confinement effects that can be exploited to tune their optical properties [11–14]. In particular, for the emerging *all-inorganic* $CsPbX_3$, nanocrystals quantum confinement affects the photoluminescence (PL) emission when the average dimensions are smaller than 5 nm ($CsPbCl_3$), 7 nm ($CsPbBr_3$) and 12 nm ($CsPbI_3$), i.e. smaller than the corresponding exciton Bohr radius.

Size and shape of nanocrystals can be controlled by varying the chemical nature of the surface ligands (i.e. capping agents used to stabilize the nanocrystals) and controlling reaction parameters such as temperature and time, in colloidal synthesis. To date, nanocrystals with a wide range of morphologies have been synthesized [15, 16], including nanocubes, nanowires, nanorods, nanoplates, nanosheets, spherical or multifaced nanocrystals, and quantum dots (i.e. nanocubes with sizes in the strong quantum-confinement regime).

The composition, size, morphology and surface functionalization of $CsPbX_3$ nanocrystals are crucial in the determination of their optoelectronic properties, and therefore their structural characterization is fundamental. Nuclear Magnetic Resonance (NMR) spectroscopy has gained an important role in this field. On one hand, nanocrystal colloidal dispersions have been investigated by solution NMR, specifically addressing the composition, conformation, and binding properties of organic ligands [17–21]. On the other hand, Solid State NMR (SSNMR) has been extensively applied to study the structure and dynamics of bulk lead halide perovskites [22–24], while only a limited number of studies have been performed on MHP nanocrystals [25–32]. In particular, very recent results have been reported concerning the surface and structural characterization of $CsPbBr_3$ nanocrystals. Noticeably, Chen et al. [28] devised an atomistic model for the surface termination of $CsPbBr_3$ nanocubes supported by $^1H\{^{133}Cs\}$ RESPDOR and $^1H\{^{207}Pb\}$ S-REDOR experiments. The power of ^{133}Cs SSNMR for the structure and surface characterization has been confirmed by Hooper et al. [32] in a study of $CsPbBr_3$ nanospheres with different diameters.

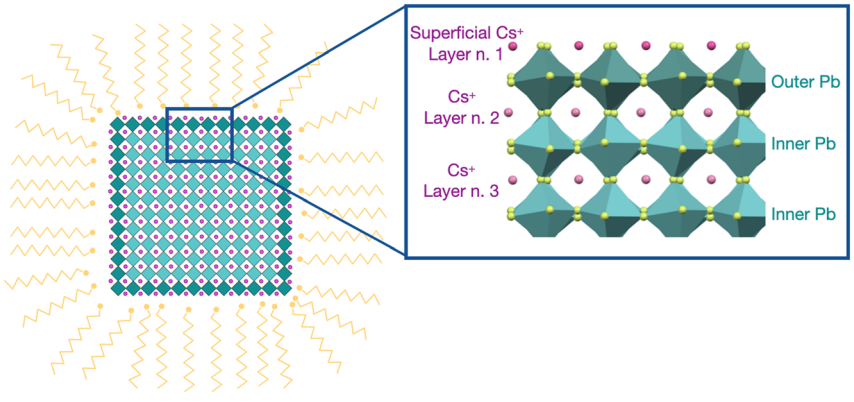

Fig. 1: Left: 2D model of a $CsPbBr_3$ NC with surface ligands. Right: ideal model of the NC's outer layers in which octahedra represent Pb^{2+} cations coordinated to Br^- anions (yellow spheres) and magenta spheres represent Cs^+ cations. The layer numbers refer to the geometrical model described in the following.

In the present work, $CsPbBr_3$ nanocubes (NCs) (Fig. 1) exhibiting quantum confinement effects were investigated by multinuclear SSNMR experiments. ^{1}H and ^{13}C SSNMR was applied to probe ligand-nanocrystals interactions, while ^{207}Pb and ^{133}Cs SSNMR was exploited to identify differences in the local chemical environment between cations residing in external and internal layers of the NCs. The investigated nanocrystals bear different ligands with respect to those reported by Chen et al. [28] and have different morphology with respect to nanospheres studied by Hooper et al. [32]. This study can be therefore considered complementary with respect to such previous reports, thus contributing to elucidating the structural features of $CsPbBr_3$ based nanomaterials.

Materials and methods

Materials

Cesium carbonate (99 %), lead acetate (99 %), benzoyl bromide (97 %), octadecene (ODE, 90 %), oleic acid (OA, 90 %), oleylamine (OLAM, 70 %), toluene (>99.7 %), dimethyl sulfoxide, cesium bromide (99.9 %), lead bromide (99.9 %), and hydrobromic acid (48 %) were supplied by Sigma Aldrich and used as received.

Synthesis of $CsPbBr_3$ nanocubes

The synthesis of **$CsPbBr_3$ NCs** was performed following the work by Imran et al. [33]. Lead acetate (304 mg) and cesium carbonate (64 mg) were mixed in 15 mL of ODE, in the presence of 1.2 mL of OA and 4 mL of OLAM. The mixture was heated for 1 h at 110 °C under vacuum to form cesium oleate. Then the temperature was raised to 170 °C under nitrogen, and 0.3 mL of benzoyl bromide was swiftly injected. The reaction mixture was immediately cooled down using an ice-water bath. 15 mL of toluene was added to the reaction mixture, and the NCs were first purified by centrifugation for 5 min at 9000 rpm. The supernatant solution was discarded, and the precipitated nanocrystals were dissolved in toluene. The bulky precipitate was removed by centrifugation at 9000 rpm for 5 min, while keeping the fraction of the NCs that remained dispersed in toluene.

Bulk $CsPbBr_3$ was synthesized by dissolving 1.9 mmol of cesium bromide and lead bromide in 3 mL of dimethyl sulfoxide and precipitated with 3 mL of HBr. Then it was dried overnight in a vacuum oven at 80 °C.

X-ray powder diffraction

X-ray Powder Diffraction (XRPD) measurements were carried out using a Bruker D8 Advance diffractometer equipped with a Cu K_α radiation and operating in Theta–Theta Bragg Brentano geometry at 40 kV and 40 mA. Lattice parameters and mean crystallite size were evaluated from a Pawley fit using the TOPAS® software (Bruker) considering the orthorhombic space group *Pnma*.

Transmission Electron Microscopy

Transmission Electron Microscopy (TEM) analysis was performed using a JEOL 100 SX microscope, operating at 100 kV. The samples were prepared by drop drying a dilute suspension of the NCs in toluene onto 200 mesh carbon-coated copper grids. The mean size, standard deviation and size distribution were obtained from statistical analysis performed over 370 NCs.

Optical characterization

The UV–Vis absorption spectra were collected at room temperature with a Cary 5000 UV–Vis-NIR spectrophotometer (Agilent). The photoluminescence spectra were measured at room temperature using an excitation wavelength of 350 nm on a Fluorolog-3 spectrofluorometer (Horiba), equipped with a 450 W xenon arc lamp, double-grating excitation and single-grating emission monochromators. Quartz Suprasil QS cuvettes (Hellma) were used for the measurements.

Solid state NMR

SSNMR experiments were performed on a Bruker Avance NEO 500 spectrometer working at Larmor Frequencies of 500.13 MHz for ^{1}H, 125.77 MHz for ^{13}C, 104.63 MHz for ^{207}Pb, and 65.50 MHz for ^{133}Cs. A triple-resonance Cross-Polarization Magic Angle Spinning (CP-MAS) probehead was used, accommodating rotors with an external diameter of 2.5 mm, with $\pi/2$ pulse durations of 2.3, 5.8, 3.4 and 10 µs for ^{1}H, ^{13}C, ^{207}Pb, and ^{133}Cs, respectively. The chemical shift was referenced to the signal of adamantane at 38.48 ppm for ^{13}C and calculated from the same value for all other nuclei, thus using the unified scale recommended by IUPAC [34]. All the MAS experiments were recorded at a spinning frequency of 15 kHz.

^{1}H MAS spectra were acquired by direct excitation (DE) accumulating 32 scans with a recycle delay of 2 s.

^{13}C MAS spectra were acquired by cross-polarization (CP) and DE experiments. CP spectra were registered using a contact time of 4 ms and accumulating 20 000 scans. DE spectra were registered using a recycle delay of 50 s and accumulating 10 000 scans.

^{207}Pb spectra were acquired using the Hahn-echo pulse sequence, under both static and MAS conditions. ^{207}Pb MAS spectra were acquired with an echo delay of 66.7 µs and a recycle delay of 0.2 s for the $CsPbBr_3$ NCs and bulk $CsPbBr_3$, accumulating 75 120 scans and 9000 scans, respectively. ^{207}Pb static spectra were acquired with an echo delay of 20 µs for the $CsPbBr_3$ NCs and of 66.7 µs for bulk $CsPbBr_3$, with a recycle delay of 1 s and accumulating 5000 scans for both samples.

^{133}Cs DE MAS spectra were acquired with a recycle delay of 120 s, accumulating 128 and 16 scans for $CsPbBr_3$ NCs and bulk $CsPbBr_3$, respectively. ^{133}Cs spin-lattice relaxation times (T_1) were measured under MAS by using the Saturation Recovery pulse sequence, with 22 variable delays ranging from 10 ms to 300 s.

Results and discussion

Nanocubes synthesis and basic characterization

$CsPbBr_3$ NCs were synthesized following a procedure developed by Imran et al. [33] based on the injection of benzoyl bromide into a hot solution (170 °C) containing cesium carbonate and lead acetate in the presence of oleic acid (OA) and oleylamine (OLAM) as surfactants and octadecene as solvent. A bulk $CsPbBr_3$ sample was also prepared in order to compare the properties of the NCs with the corresponding bulk material.

The NC dispersion in toluene was first characterized through electron microscopy (TEM) and optical spectroscopy. TEM investigation reveals the presence of cubic nanocrystals with relatively sharp size distribution (Fig. 2a and b). The mean size obtained through statistical analysis of TEM images is 12.3 nm (dimension of the diagonal of square projection, corresponding to an edge dimension of 8.8 nm), with a standard deviation of 1.6 nm. The UV–Vis absorption spectrum features an excitonic peak at 2.46 eV, while the emission peak in the photoluminescence spectrum displays a Stokes shift of 33 meV (Fig. 2c). Given the size of our NCs, the observed Stokes shift is consistent with previous studies performed on cubic nanocrystals as a function of their size [11, 12]. The emission peak has a relatively low full width at half maximum (76 meV).

In order to perform X-ray powder diffraction (XRPD) and SSNMR investigations, the NCs were dried under vacuum and reduced into a powder. The diffraction pattern of the NCs powder displays significantly broader

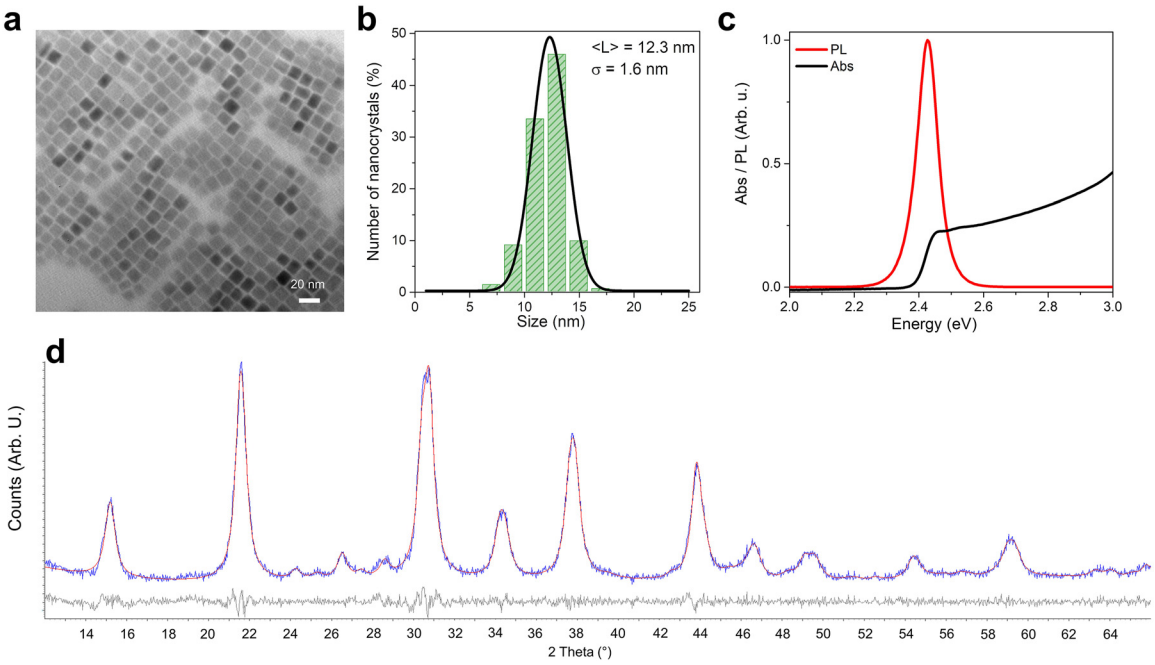

Fig. 2: TEM, UV–Vis absorption, photoluminescence, and XRPD of the synthesized $CsPbBr_3$ NCs: (a) representative TEM image of the synthesized NCs and (b) statistical size distribution obtained from the analysis of TEM images, with the Gaussian fit reported as a black line; the reported size is referred to the diagonal of the square face of the cube. (c) Absorption (black line) and photoluminescence (red line) spectra of a diluted dispersion of the NCs in toluene. (d) Experimental X-ray powder diffraction pattern (collected using Cu K_α X-ray source) of the NCs (blue curve) and Pawley fitting (red curve) of the experimental curve using TOPAS software and the orthorhombic crystal structure (*Pnma* space group); the gray curve represents the residuals of the fitting.

diffraction peaks with respect to that of bulk $CsPbBr_3$ (Fig. 3), consistent with the reduced size of the NCs. Even though the orthorhombic phase is the thermodynamically stable form of $CsPbBr_3$ at room temperature [35], sometimes non-equilibrium phases can be obtained in nanocrystal synthesis [36, 37]. The discrimination between cubic and orthorhombic phases in $CsPbBr_3$ nanocrystals is often challenging due to several effects [38, 39]. First, the small size of the particles is responsible for the broadening of the diffraction peaks, thus complicating the discrimination between the two phases that have a similar diffraction pattern [40]. Secondly, sometimes the large amount of surfactants needed to stabilize small NCs in solution causes a large background signal, complicating the analysis of the diffraction pattern. Finally, due to the cubic shape of the nanocrystals, preferential orientation of the crystallites typically occurs when they are drop-casted on a flat sample holder, thus exposing only a set of crystallographic planes. To avoid the latter effect, we analyzed the NCs powder after drying and grinding it to ensure random orientation of the crystallites. For both the bulk sample and the NCs we found that the XRPD pattern matches very well the orthorhombic phase (Fig. 3). To further confirm this, we performed a Pawley fit (Fig. 2d) of the diffraction pattern, finding an excellent agreement with the orthorhombic space group (*Pnma*). The *a*, *b* and *c* lattice parameters determined through the fitting were 8.19044(84) Å, 11.75199(80) Å, and 8.243490(7) Å, respectively, for the NCs. The prevalence of the orthorhombic phase is in agreement with previous results on $CsPbBr_3$ NCs with similar size and prepared with similar synthetic methods [28, 39]. The average crystallite size determined through the fit and using *Sherrer* equation was 15.4 nm, which is in reasonable agreement with the size determined by TEM analysis, highlighting that the NCs are monocrystalline. As far as the bulk sample is concerned, the Pawley fit of the diffraction pattern using the *Pnma* orthorhombic space group revealed *a*, *b*, and *c* lattice parameters of 8.20885(15) Å, 11.7617(2) Å, and 8.25835(18) Å, respectively. The fit also gave an estimate of the mean crystallite size, which was found to be 560(20) nm, consistently with a bulk sample.

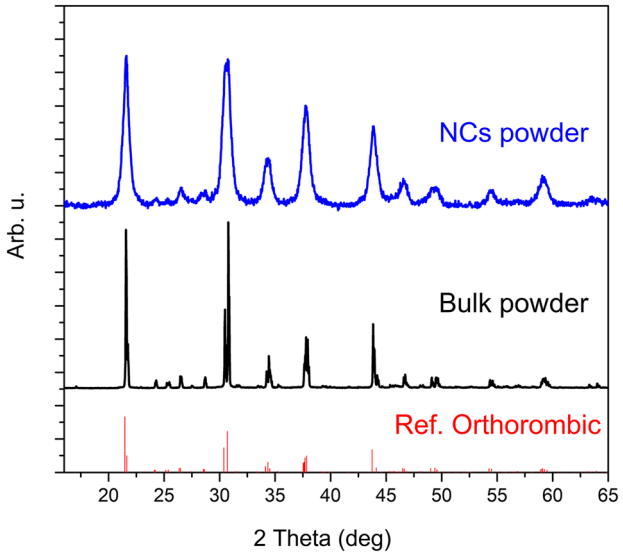

Fig. 3: Comparison between the powder X-ray diffraction pattern of the bulk $CsPbBr_3$ powder (black line) and the $CsPbBr_3$ NCs powder (blue line). Cu K_α radiation (1.54 Å) is used as the X-ray source. The reference pattern of the orthorhombic phase (PDF 04-014-9676) is shown (red line) for the sake of comparison.

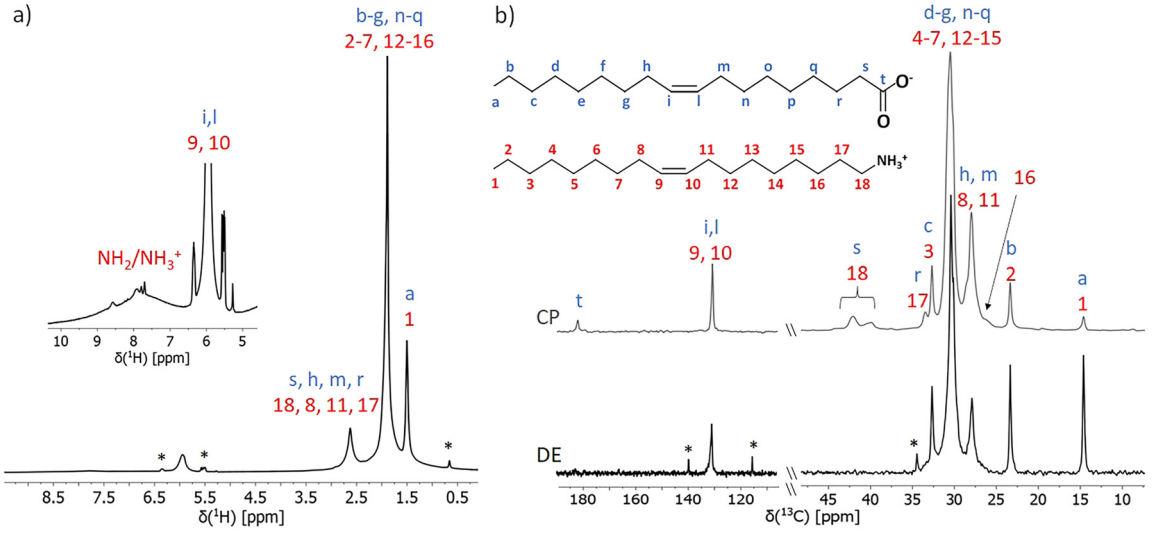

Fig. 4: (a) ^{1}H MAS and (b) ^{13}C CP and DE MAS NMR spectra of $CsPbBr_3$ NCs with spectral assignment. Inset in (a) is an expansion of the region 4.5–10 ppm. Asterisks indicate signals from residual 1-octadecene.

SSNMR characterization

^{1}H and ^{13}C NMR spectra

In order to investigate the ligands and their interaction with $CsPbBr_3$ NCs, we recorded ^{1}H and ^{13}C high-resolution SSNMR spectra. Resonances arising from the aliphatic chains of OA and OLAM were observed and assigned (Fig. 4).

In the ^{1}H MAS spectrum, the most intense signals (Fig. 4a) are those corresponding to the alkyl protons of both OA and OLAM, observed in the range 0.6–3 ppm. Olefinic protons resonate at about 6 ppm and show higher chemical shift and broader lines with respect to those observed for free OLAM and OA in solution (≈5.2–5.4 ppm) [41, 42], suggesting that olefinic groups interact with NCs surface. On one hand, the absence of signals above 10 ppm indicates that oleic acid is completely deprotonated. On the other hand, a broad peak is

observed in the 7.5–8 ppm region, which can be assigned to both protons of $–NH_2$ and $–NH_3^+$ groups, indicating that protonation of OLAM occurred. Since the only source of protons is constituted by OA, considering the nominal OA/OLAM molar ratio, the protonation of OLAM should be partial, unless all the non-protonated OLAM is removed during the NC preparation. Indeed, chemical shift values of about 8 ppm have also been reported for $–NH_2$ protons coordinated to cations at the surface of metallic nanoparticles [43]. The very broad signal is therefore compatible with the presence of both $–NH_3^+$ and $–NH_2$ groups interacting with the NCs surface. The observed chemical shifts are in agreement with previously reported values [41, 44] and indicate that OLAM $–NH_2$ groups are coordinated with Cs^+, while $–NH_3^+$ groups can be coordinated to halides on the nanocrystal surface or can substitute superficial Cs^+ cations, as reported in a previous solution state NMR study [19]. Evidence of ammonium ions coordinating to superficial halides and substituting Cs^+ cations has been reported in the case of dodecylammonium ligands of $CsPbBr_3$ NCs [28].

The ^{13}C MAS spectra, acquired by cross-polarization (CP) and direct excitation (DE) experiments (Fig. 4b), show the signals of carbons in the alkyl chains in the 14–40 ppm range. In particular, the inner-chain methylene carbons resonate at about 30.4 ppm. This chemical shift value indicates a certain degree of inter-conformational mobility of the alkyl chains, since it corresponds to an average between the chemical shifts of chains in the rigid all-trans arrangement (≈33 ppm) and the gauche conformation (≈30 ppm) [45, 46]. The chemical shift of the terminal methyl group, at 14.6 ppm, similar to that of pure OLAM (about 14 ppm) and OA (about 15.5 ppm) [47] and higher than values reported for methyl's in monolayers of amphiphilic molecules (12.5–13 ppm) [46], is compatible with the presence of aliphatic multilayers in disordered environments, thus suggesting the presence of interactions between methyl groups of neighbor NCs.

From a comparison of the signals present in the CP and DE NMR spectra and their corresponding intensities, we can get an indication of the relative rigidity of different fragments of the OLAM and OA chains: CP experiments rely on ^1H–^{13}C dipolar couplings and give enhanced signals for rigid moieties, while DE spectra show signals from ^{13}C nuclei with longitudinal relaxation time (T_1) values sensibly shorter than the used recycle delay (50 s), mainly associated with high-mobility environments. In particular, the signals of carbons 18 and s (peaks at 39 and 42 ppm) and carbon t (peak at 181 ppm) are observed only in the CP spectrum, indicating a more restricted mobility for the polar heads of OA and OLAM due to their coordination to the nanocrystal surface, thus confirming ^1H NMR results in the case of OLAM/oleylammonium. In addition, the reduced intensity of the methyl signal in the CP with respect to the DE spectrum confirms that the chain terminations are subjected to a higher mobility.

^{207}Pb NMR spectra

^{207}Pb is a 22 % abundant nuclear spin I = 1/2 isotope with receptivity 12 times higher than that of ^{13}C. These characteristics allow a relatively easy observation of lead in bulk perovskite samples, despite the very large line width. For perovskite nanocrystals, the sensitivity is lower with respect to bulk samples because of the lower concentration of Pb atoms in the sample, and 5–10 times more transients are needed to obtain a similar signal to noise ratio. ^{207}Pb MAS spectra were acquired on both $CsPbBr_3$ NCs and bulk $CsPbBr_3$ (Fig. 5a and b). The spectrum of bulk $CsPbBr_3$ shows a broad signal centered at 255 ppm characterized by a multiplet pattern resulting from the J-coupling between ^{207}Pb and the six quadrupolar $^{79/81}Br$ nuclei (I = 3/2) in the octahedral coordination [25]. The broad ^{207}Pb signal of $CsPbBr_3$ NCs is shifted (at 237 ppm) with respect to the signal of bulk $CsPbBr_3$ and no fine structure can be observed, in agreement with previously reported data [25, 27, 28, 32].

The line shape of the ^{207}Pb signal of $CsPbBr_3$ NCs has been previously explained by the higher disorder associated with particle size reduction and higher ion mobility in NCs with respect to bulk perovskite [25]. Here we want to investigate the additional possible differences of isotropic and anisotropic chemical shift of ^{207}Pb near to the surface and in the inner part of the NCs. Chemical Shift Anisotropy (CSA) has been previously reported to be appreciable for the outer lead nuclei in 2D Ruddlesden-Popper (RP) perovskites, while the inner lead atoms (present when the number of perovskite layers is higher than two) exhibit a negligible CSA [48], as reported for 3D lattices [49, 50]. In NCs we can hypothesize that ^{207}Pb nuclei in the first layer near the surface (outer Pb in Fig. 1) can have a chemical environment, and therefore isotropic and anisotropic chemical shift,

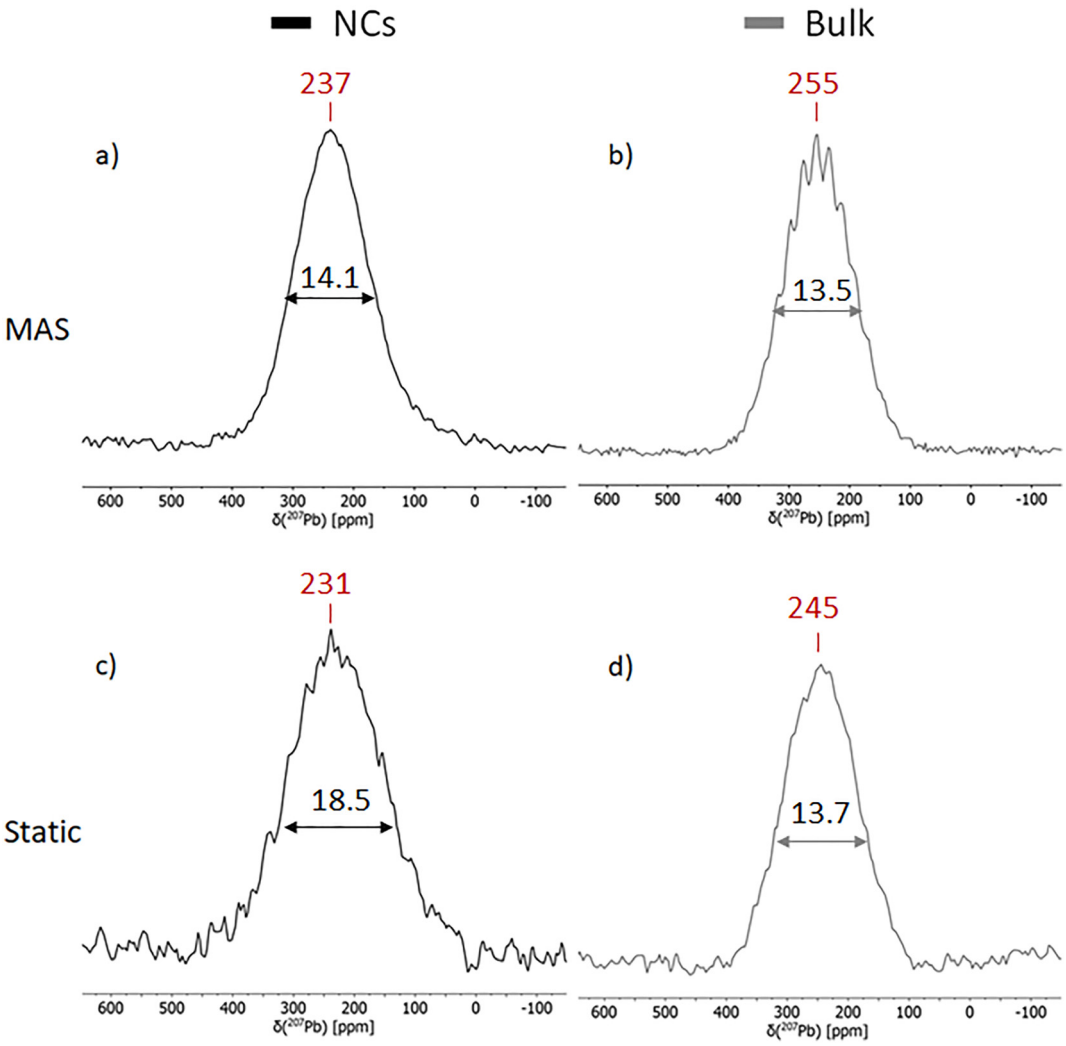

Fig. 5: ^{207}Pb Hahn Echo NMR spectra of $CsPbBr_3$ NCs (a and c) and bulk $CsPbBr_3$ (b and d). Spectra reported in (a) and (b) were registered under MAS, while spectra in (c) and (d) were registered in static conditions. Chemical shift (ppm) and line width at half height (kHz) are indicated for each signal.

similar to those in the outer layers of 2D RP phases, while the core ^{207}Pb nuclei are in a bulk-like environment. This hypothesis can be supported by comparing MAS (Fig. 5a and b) and static (Fig. 5c and d) ^{207}Pb NMR spectra: while the static spectrum of bulk $CsPbBr_3$ has a line width similar to the corresponding MAS spectrum, in the case of NCs we observe a significant reduction of the line width (from 18.5 to 14.1 kHz) in passing from the static to the MAS spectrum. A peculiar CSA shape is not observed, but this can be due to the superposition of signals with different CSA values and disorder due to defects. According to the simple geometrical model described in the following, we can estimate that the lead atoms in the outer layer of the nanocrystals are in a non-negligible amount (about 35 % of the total). This observation is compatible with a superposition of at least two different signals with different isotropic and anisotropic chemical shift values, the latter contributing only to the static spectrum.

^{133}Cs NMR spectra and relaxation times T_1

^{133}Cs is a 100 % abundant nucleus with spin I = 7/2, a small quadrupole moment and a chemical shift that spans over a relatively wide range of frequencies (~500 ppm), which makes it very sensitive to even subtle differences in

the local environment. For all these reasons, ^{133}Cs is a suitable nucleus for probing the atomic-level structure of $CsPbBr_3$ materials [24]. Given the small quadrupole moment and the relatively high symmetry of perovskites lattices, it has been shown that in MAS experiments the quadrupole interaction and CSA are negligible, and the position of the peaks can be interpreted in terms of isotropic chemical shifts ($\delta(^{133}Cs)$).

The ^{133}Cs DE MAS spectrum of bulk $CsPbBr_3$ (Fig. 6) shows a single signal centered at 122.4 ppm, in agreement with previously reported values [27, 32, 51]. It is worth noticing that two different referencing methods are used in the literature. Here the IUPAC referencing [34] is used and chemical shift values from refs [28, 51], referenced using $\delta(^{133}Cs)$ = 0 ppm for 1 M aqueous CsCl, must be shifted by +13 ppm to be consistent with ours. The ^{133}Cs DE MAS spectrum of $CsPbBr_3$ NCs (Fig. 6) shows a main signal with an asymmetrical line shape spanning from about 70 to 130 ppm, and two broad, low intensity and partially overlapped signals centered at 163 and 185 ppm. The peak at 163 ppm can be ascribed to the Cs nuclei coordinated to the amine group of the non-protonated OLAM ligands or Cs nuclei adjacent to oleyl ammonium cations substituting Cs^+ ions, as this resonance has previously been assigned to Cs nuclei close to didodecyldimethyl ammonium groups [31]. We can therefore assign the signal at 185 ppm to Cs nuclei coordinated to the OA carboxylate groups. The line shape of the main signal can be deconvoluted by applying a spectral fitting procedure using the minimum number of peaks. A very good line shape reproduction is obtained with the use of three Gaussian peaks centered at 99.0, 111.0 and 116.4 ppm, which get narrower with increasing chemical shift. As already suggested by Hooper et al. [32] for $CsPbBr_3$ nanospheres, each peak may represent different NC layers, with the chemical shift increasing from the surface to the NC core. The line width trend most probably reflects a larger distribution of local environments as the surface is gradually approached, mainly due to the interactions with ligands and the higher concentration of vacancies and lattice distortions near the surface. No signal is observed at the chemical shift of bulk $CsPbBr_3$, indicating the absence of large bulk-like nanoparticles in the sample and thus testifying to a good stabilization of the NCs.

By applying a simple geometric model, we can hypothesize a connection between the relative integral intensities of each peak and the number of Cs atoms in the corresponding layers of the NCs. In this model we assume that: (i) the NCs have a perfectly cubic structure with a side equal to the average size found by electron microscopy (8.8 nm); (ii) the surface of the NCs is Cs terminated as reported by Chen et al. [28]; (iii) the Cs nuclei are equally spaced within the particle at a distance of 5.9 Å (measured from XRD structure in Ref. [39]); (iv) no vacancies are present at the A sites. This results in each NC made of 4096 Cs atoms, distributed over 8 different layers, that will be numbered from 1 to 8 going from the surface to the core of the NC.

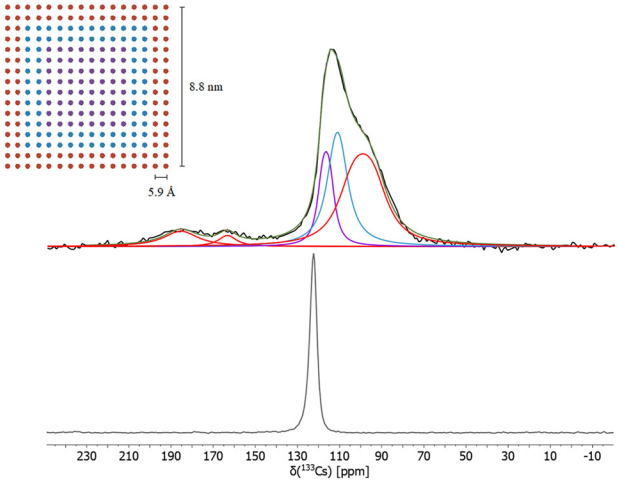

Fig. 6: ^{133}Cs DE MAS NMR spectrum of $CsPbBr_3$ NCs (top) and bulk $CsPbBr_3$ (bottom). Top: the experimental spectrum (black), the total line arising from the deconvolution procedure (green) and the single Gaussian peaks corresponding to different layers of the NPs (red, blue and purple) are reported. A schematic representation of a bidimensional section of the cubic model used in the spectrum interpretation is also reported, with colored dots corresponding to Cs nuclei in the layers associated with the single resonances.

Table 1: Isotropic chemical shifts, relative integrals and spin lattice relaxation times (T_1), measured at 298 K, of the different resonances obtained from the deconvolution of the ^{133}Cs DE MAS NMR spectrum of $CsPbBr_3$ NCs, layer numbers (geometric model described in the text and inset of Fig. 6) and relative weights of Cs atoms in the layers associated with the different resonances.

^{133}Cs MAS NMR spectrum			Geometrical Model	
δ [ppm]	Relative integral [%]	T_1 [s]	Layer n.	Relative weight [%]
116.4	15.9	14.1	5, 6, 7, 8	12.5
111.0	30.1	9.0	3, 4	29.7
99.0	46.0 ┐	2.9		
163.0	3 ├ 54	-	1, 2	57.8
185.0	5 ┘	-		

As can be seen in Table 1, there is a good agreement between the experimental integral intensities obtained from the spectral deconvolution and the relative weights of Cs nuclei belonging to the different layers of the NCs derived from the geometric model if we take the external shell as made of two Cs layers, the inner core by 4 Cs layers, and the intermediate region by 2 Cs layers. Moreover, considering that the concentration of vacancies increases as the surface is gradually approached, the relative weight of the Cs nuclei in the two outer layers is probably slightly overestimated in the geometric model.

Spin-lattice relaxation times, T_1, were measured at 298 K for ^{133}Cs nuclei corresponding to the three components of the main signal. In all cases a monoexponential longitudinal magnetization recovery was observed and T_1 values considerably lower than those reported in the literature for bulk $CsPbBr_3$ (>100 s) [52] were determined, as shown in Table 1.

The component at 116.4 ppm, ascribed to the innermost fraction of Cs nuclei, has the longest spin-lattice relaxation time (14.1 s), while the component at 99.0 ppm – Cs nuclei closest to the surface – is characterized by the shortest T_1 (2.9 s). The intermediate component centered at 111.0 ppm shows an intermediate T_1 value (9.0 s). These values are similar to those found for spherical $CsPbBr_3$ nanoparticles [32] with a volume comparable to those of the NCs here studied. The decreasing trend of the T_1 values observed going from the inner core to the external NC surface can be explained by considering the greater distribution of local environments in the outer layers compared to the inner ones. Near the surface, the greater disorder may allow more relaxation mechanisms to occur, as for example those involving the modulation of the heteronuclear dipolar couplings established with the hydrogens of the mobile alkyl chains, and/or the modulation of the chemical shift anisotropy or quadrupolar couplings, which are expected to be greater in the outer layers of the nanoparticles where the symmetry breaks.

Conclusions

In this work, $CsPbBr_3$ nanocubes were synthesized and characterized by XRPD, TEM, UV–Vis, PL and SSNMR in comparison to bulk $CsPbBr_3$. The formation of nanocubes with an average side length of 8.8 nm resulted from TEM analysis, and the Stokes shift observed in the PL spectrum is compatible with this size. XRPD indicated that the obtained NCs have an orthorhombic *Pnma* crystalline structure. Multinuclear SSNMR was exploited to characterize structural features of the perovskite cubic NCs and their organic ligands. ^{13}C and ^{1}H MAS NMR spectra indicated a complete deprotonation of the oleic acid and a corresponding partial protonation of oleylamine used as ligand. Chemical shifts and line width of diagnostic signals evidenced interactions of ammonium/amine, carboxylate and olefinic groups with the $CsPbBr_3$ surface. The comparison between static and MAS ^{207}Pb NMR spectra suggested a possible contribution of chemical shift anisotropy to lead signal coming from ^{207}Pb nuclei in the outer layer of the nanocubes. This contribution, in addition to previously discussed effects of increased disorder and ion mobility, can explain the differences between ^{207}Pb NMR spectra of NCs and bulk $CsPbBr_3$. Finally, ^{133}Cs spectral and relaxation properties, discussed considering recent findings on

$CsPbBr_3$ nanocrystals with different morphology, allowed the distinction of Cs nuclei at different depths from the surface of the NCs.

Acknowledgment: Dr. Elvira Fantechi and Dr. Laura Chelazzi (Centro di Cristallografia Strutturale, University of Florence) are acknowledged for their help in X-ray Powder Diffraction analysis. Dr. Paolo Lucchesi (CIME, University of Pisa) is acknowledged for his assistance in TEM analysis. CISUP (Centre for Instrument Sharing–University of Pisa) is acknowledged for the use of the Bruker Avance Neo 500 Solid State NMR Spectrometer.
Research funding: A. G. and F. P. acknowledge the support of Italian Ministry of Education and Research (MIUR) through PRIN Project 2017CR5WCH Q-CHISS. A. P. and M. G. acknowledge the support of "Regione Toscana" through COLOURS project, POR FESR 2014–2020, grant no. 3553.04032020.158000411.

References

[1] A.S. Bhalla, R. Guo, R. Roy. *Mater. Res. Innov.* **4**, 3 (2000), https://doi.org/10.1007/s100190000062.
[2] K. Wang, D. Yang, C. Wu, M. Sanghadasa, S. Priya. *Prog. Mater. Sci.* **106**, 100580 (2019), https://doi.org/10.1016/j.pmatsci.2019.100580.
[3] Z. Wang, Z. Shi, T. Li, Y. Chen, W. Huang. *Angew. Chem., Int. Ed.* **56**, 1190 (2016), https://doi.org/10.1002/anie.201603694.
[4] A.F. Akbulatov, S.Y. Luchkin, L.A. Frolova, N.N. Dremova, K.L. Gerasimov, I.S. Zhidkov, D.V. Anokhin, E.Z. Kurmaev, K.J. Stevenson, P.A. Troshin. *J. Phys. Chem. Lett.* **8**, 1211 (2017), https://doi.org/10.1021/acs.jpclett.6b03026.
[5] D. Yang, M. Cao, Q. Zhong, P. Li, X. Zhang, Q. Zhang. *J. Mater. Chem. C* **7**, 757 (2019), https://doi.org/10.1039/c8tc04381g.
[6] Z. Wei, J. Xing. *J. Phys. Chem. Lett.* **10**, 3035 (2019), https://doi.org/10.1021/acs.jpclett.9b00277.
[7] K. Wang, S. Wang, S. Xiao, Q. Song. *Adv. Opt. Mater.* **6**, 1800278 (2018), https://doi.org/10.1002/adom.201800278.
[8] A. Privitera, M. Righetto, F. Cacialli, M.K. Riede. *Adv. Opt. Mater.* **9**, 2100215 (2021), https://doi.org/10.1002/adom.202100215.
[9] M. Hao, Y. Bai, S. Zeiske, L. Ren, J. Liu, Y. Yuan, N. Zarrabi, N. Cheng, M. Ghasemi, P. Chen, M. Lyu, D. He, J.H. Yun, Y. Du, Y. Wang, S. Ding, A. Armin, P. Meredith, G. Liu, H.M. Cheng, L. Wang. *Nat. Energy* **5**, 79 (2020), https://doi.org/10.1038/s41560-019-0535-7.
[10] N.S. Peighambardoust, E. Sadeghi, U. Aydemir. *ACS Appl. Nano Mater.* **5**, 14092 (2022), https://doi.org/10.1021/acsanm.2c02787.
[11] M.C. Brennan, J.E. Herr, T.S. Nguyen-Beck, J. Zinna, S. Draguta, S. Rouvimov, J. Parkhill, M. Kuno. *J. Am. Chem. Soc.* **139**, 12201 (2017), https://doi.org/10.1021/jacs.7b05683.
[12] M.C. Brennan, J. Zinna, M. Kuno. *ACS Energy Lett.* **2**, 1487 (2017), https://doi.org/10.1021/acsenergylett.7b00383.
[13] J. Shamsi, A.S. Urban, M. Imran, L. de Trizio, L. Manna. *Chem. Rev.* **119**, 3296 (2019), https://doi.org/10.1021/acs.chemrev.8b00644.
[14] A. Dey, J. Ye, A. De, E. Debroye, S.K. Ha, E. Bladt, A.S. Kshirsagar, Z. Wang, J. Yin, Y. Wang, L.N. Quan, F. Yan, M. Gao, X. Li, J. Shamsi, T. Debnath, M. Cao, M.A. Scheel, S. Kumar, J.A. Steele, M. Gerhard, L. Chouhan, K. Xu, X. Wu, Y. Li, Y. Zhang, A. Dutta, C. Han, I. Vincon, A.L. Rogach, A. Nag, A. Samanta, B.A. Korgel, C.-J. Shih, D.R. Gamelin, D.H. Son, H. Zeng, H. Zhong, H. Sun, H.V. Demir, I.G. Scheblykin, I. Mora-Seró, J.K. Stolarczyk, J.Z. Zhang, J. Feldmann, J. Hofkens, J.M. Luther, J. Pérez-Prieto, L. Li, L. Manna, M.I. Bodnarchuk, M.V. Kovalenko, M.B.J. Roeffaers, N. Pradhan, O.F. Mohammed, O.M. Bakr, P. Yang, P. Müller-Buschbaum, P.V. Kamat, Q. Bao, Q. Zhang, R. Krahne, R.E. Galian, S.D. Stranks, S. Bals, V. Biju, W.A. Tisdale, Y. Yan, R.L.Z. Hoye, L. Polavarapu. *ACS Nano* **15**, 10775 (2021), https://doi.org/10.1021/acsnano.0c08903.
[15] X. Kong, H. Yu, F. Xu, L. Liu, Y. Wu, B. Cao. *ACS Appl. Nano Mater.* **5**, 12395 (2022), https://doi.org/10.1021/acsanm.2c03101.
[16] A.A.M. Brown, N. Mathews, P. Vashishtha, T.J.N. Hooper, Y.F. Ng, G.V. Nutan, Y. Fang, D. Giovanni, J.N. Tey, L. Jiang, B. Damodaran, T.C. Sum, S.H. Pu, S.G. Mhaisalkar. *Chem. Mater.* **33**, 2387 (2021), https://doi.org/10.1021/acs.chemmater.0c04569.
[17] A.A.M. Brown, T.J.N. Hooper, S.A. Veldhuis, X.Y. Chin, A. Bruno, P. Vashishtha, J.N. Tey, L. Jiang, B. Damodaran, S.H. Pu, S.G. Mhaisalkar, N. Mathews. *Nanoscale* **11**, 12370 (2019), https://doi.org/10.1039/c9nr02566a.
[18] R. Begum, X.Y. Chin, B. Damodaran, T.J.N. Hooper, S. Mhaisalkar, N. Mathews. *ACS Appl. Nano Mater.* **3**, 1766 (2020), https://doi.org/10.1021/acsanm.9b02450.
[19] V.K. Ravi, P.K. Santra, N. Joshi, J. Chugh, S.K. Singh, H. Rensmo, P. Ghosh, A. Nag. *J. Phys. Chem. Lett.* **8**, 4988 (2017), https://doi.org/10.1021/acs.jpclett.7b02192.
[20] D. Quarta, M. Imran, A.L. Capodilupo, U. Petralanda, B. van Beek, F. de Angelis, L. Manna, I. Infante, L. de Trizio, C. Giansante. *J. Phys. Chem. Lett.* **10**, 3715 (2019), https://doi.org/10.1021/acs.jpclett.9b01634.
[21] F. Aiello, S. Masi. *J. Nanomater.* **11**, 2024 (2021), https://doi.org/10.3390/nano11082024.
[22] W.M.J. Franssen, A.P.M. Kentgens. *Solid State Nucl. Magn. Reson.* **100**, 36 (2019), https://doi.org/10.1016/j.ssnmr.2019.03.005.
[23] L. Piveteau, V. Morad, M.V. Kovalenko. *J. Am. Chem. Soc.* **142**, 19413 (2020), https://doi.org/10.1021/jacs.0c07338.
[24] D.J. Kubicki, S.D. Stranks, C.P. Grey, L. Emsley. *Nat. Rev. Chem.* **5**, 624 (2021), https://doi.org/10.1038/s41570-021-00309-x.
[25] M. Aebli, L. Piveteau, O. Nazarenko, B.M. Benin, F. Krieg, R. Verel, M.V. Kovalenko. *Sci. Rep.* **10**, 8229 (2020), https://doi.org/10.1038/s41598-020-65071-4.

[26] A. Ray, D. Maggioni, D. Baranov, Z. Dang, M. Prato, Q.A. Akkerman, L. Goldoni, E. Caneva, L. Manna, A.L. Abdelhady. *Chem. Mater.* **31**, 7761 (2019), https://doi.org/10.1021/acs.chemmater.9b02944.
[27] A. Karmakar, M.S. Dodd, X. Zhang, M.S. Oakley, M. Klobukowski, V.K. Michaelis. *Chem. Comm.* **55**, 5079 (2019), https://doi.org/10.1039/c8cc09622h.
[28] Y. Chen, S.R. Smock, A.H. Flintgruber, F.A. Perras, R.L. Brutchey, A.J. Rossini. *J. Am. Chem. Soc.* **142**, 6117 (2020), https://doi.org/10.1021/jacs.9b13396.
[29] P. Vashishtha, T.J.N. Hooper, Y. Fang, D. Kathleen, D. Giovanni, M. Klein, T.C. Sum, S.G. Mhaisalkar, N. Mathews, T. White. *Nanoscale* **13**, 59 (2021), https://doi.org/10.1039/d0nr08093d.
[30] P. Vashishtha, S.A. Veldhuis, S.S.H. Dintakurti, N.L. Kelly, B.E. Griffith, A.A.M. Brown, M.S. Ansari, A. Bruno, N. Mathews, Y. Fang, T. White, S.G. Mhaisalkar, J.V. Hanna. *J. Mater. Chem. C* **8**, 11805 (2020), https://doi.org/10.1039/d0tc02038a.
[31] J. Shamsi, D. Kubicki, M. Anaya, Y. Liu, K. Ji, K. Frohna, C.P. Grey, R.H. Friend, S.D. Stranks. *ACS Energy Lett.* **5**, 1900 (2020), https://doi.org/10.1021/acsenergylett.0c00935.
[32] T.J.N. Hooper, Y. Fang, A.A.M. Brown, S.H. Pu, T.J. White. *Nanoscale* **13**, 15770 (2021), https://doi.org/10.1039/d1nr04602k.
[33] M. Imran, V. Caligiuri, M. Wang, L. Goldoni, M. Prato, R. Krahne, L. de Trizio, L. Manna. *J. Am. Chem. Soc.* **140**, 2656 (2018), https://doi.org/10.1021/jacs.7b13477.
[34] R.K. Harris, E.D. Becker, S.M. Cabral De Menezes, P. Granger, R.E. Hoffman, K.W. Zilm. *Pure Appl. Chem.* **80**, 59 (2008), https://doi.org/10.1016/j.ssnmr.2008.02.004.
[35] C.C. Stoumpos, C.D. Malliakas, J.A. Peters, Z. Liu, M. Sebastian, J. Im, T.C. Chasapis, A.C. Wibowo, D.Y. Chung, A.J. Freeman, B.W. Wessels, M.G. Kanatzidis. *Cryst. Growth Des.* **13**, 2722 (2013), https://doi.org/10.1021/cg400645t.
[36] S. Toso, Q.A. Akkerman, B. Martín-García, M. Prato, J. Zito, I. Infante, Z. Dang, A. Moliterni, C. Giannini, E. Bladt, I. Lobato, J. Ramade, S. Bals, J. Buha, D. Spirito, E. Mugnaioli, M. Gemmi, L. Manna. *J. Am. Chem. Soc.* **142**, 10198 (2020), https://doi.org/10.1021/jacs.0c03577.
[37] Y. Vasquez, Z. Luo, R.E. Schaak. *J. Am. Chem. Soc.* **130**, 11866 (2008), https://doi.org/10.1021/ja804858u.
[38] M.C. Brennan, M. Kuno, S. Rouvimov. *Inorg. Chem.* **58**, 1555 (2019), https://doi.org/10.1021/acs.inorgchem.8b03078.
[39] P. Cottingham, R.L. Brutchey. *Chem. Comm.* **52**, 5246 (2016), https://doi.org/10.1039/c6cc01088a.
[40] C.F. Holder, R.E. Schaak. *ACS Nano* **13**, 7359 (2019), https://doi.org/10.1021/acsnano.9b05157.
[41] S.R. Smock, T.J. Williams, R.L. Brutchey. *Angew. Chem.* **130**, 11885 (2018), https://doi.org/10.1002/anie.201806916.
[42] F. Liu, Y. Zhang, C. Ding, S. Kobayashi, T. Izuishi, N. Nakazawa, T. Toyoda, T. Ohta, S. Hayase, T. Minemoto, K. Yoshino, S. Dai, Q. Shen. *ACS Nano* **11**, 10373 (2017), https://doi.org/10.1021/acsnano.7b05442.
[43] X. Lu, M.S. Yavuz, H.Y. Tuan, B.A. Korgel, Y. Xia. *J. Am. Chem. Soc.* **130**, 8900 (2008), https://doi.org/10.1021/ja803343m.
[44] Q. Zhong, M. Cao, Y. Xu, P. Li, Y. Zhang, H. Hu, D. Yang, Y. Xu, L. Wang, Y. Li, X. Zhang, Q. Zhang. *Nano Lett.* **19**, 4151 (2019), https://doi.org/10.1021/acs.nanolett.9b01666.
[45] S. Borsacchi, M. Geppi, L. Ricci, G. Ruggeri, C.A. Veracini. *Langmuir* **23**, 3953 (2007), https://doi.org/10.1021/la063040a.
[46] W. Gao, L. Dickinson, C. Grozinger, F.G. Morin, L. Reven. *Langmuir* **12**, 6429 (1996), https://doi.org/10.1021/la9607621.
[47] K.J. Crowley, R.T. Forbes, P. York, D.C. Apperley, H. Nyqvist, O. Camber. *J. Pharm. Sci.* **89**, 1286 (2000), https://doi.org/10.1002/1520-6017(200010)89:10<1286::aid-jps6>3.0.co;2-o.
[48] J. Lee, W. Lee, K. Kang, T. Lee, S.K. Lee. *Chem. Mater.* **33**, 370 (2021), https://doi.org/10.1021/acs.chemmater.0c04078.
[49] B.A. Rosales, L. Men, S.D. Cady, M.P. Hanrahan, A.J. Rossini, J. Vela. *Chem. Mater.* **28**, 6848 (2016), https://doi.org/10.1021/acs.chemmater.6b01874.
[50] W.M.J. Franssen, S.G.D. van Es, R. Dervişoğlu, G.A. de Wijs, A.P.M. Kentgens. *J. Phys. Chem. Lett.* **8**, 61 (2017), https://doi.org/10.1021/acs.jpclett.6b02542.
[51] D.J. Kubicki, D. Prochowicz, A. Hofstetter, S.M. Zakeeruddin, M. Grätzel, L. Emsley. *J. Am. Chem. Soc.* **139**, 14173 (2017), https://doi.org/10.1021/jacs.7b07223.
[52] D.J. Kubicki, D. Prochowicz, A. Pinon, G. Stevanato, A. Hofstetter, S.M. Zakeeruddin, M. Grätzel, L. Emsley. *J. Mater. Chem. A* **7**, 2326 (2019), https://doi.org/10.1039/c8ta11457a.